# Ultra-high efficient pH induced selective removal of cationic and anionic dyes from complex coexisted solution by novel amphoteric biocomposite microspheres

# Ultra-high efficient pH induced selective removal of cationic and anionic dyes from complex coexisted solution by novel amphoteric biocomposite microspheres

Bingjie Wang[a], Xiaoyong Yang[a], Liang Ma[a], Linlin Zhai[a], Jin Xuan[b], Changjun Liu[a], Zhishan Bai[a,*]

[a] State Environmental Protection Key Laboratory of Environmental Risk Assessment and Control on Chemical Process, School of Mechanical and Power Engineering, East China University of Science and Technology, Shanghai 200237, P. R. China

[b] Department of Chemical Engineering, Loughborough University, Loughborough, LE11 3TU, United Kingdom

[*] Corresponding Authors, Email address: baizs@ecust.edu.cn. Tel: +86 (021) 64253693; Fax: +86 (021) 64253693.

**Abstract:**

The substandard discharge of highly toxic dyestuff wastewater will pose a serious threat to the environment and human beings, even causing unimaginable irreversible damages. In the current study, novel amphoteric carboxymethyl chitosan/gelatin microspheres (CCGMs), synthesized by a facile inverse suspension route with two-step successive crosslinking process, were evaluated as a potential adsorbent for high efficient pH induced selective removal of azo-dyes. The as-prepared CCGMs were characterized using scanning electron microscopy (SEM), Fourier transform infrared spectroscopy (FT-IR), thermogravimetry analysis (TGA) and X-ray photoelectron spectroscopy (XPS). Various influential factors such as solution pH, temperature, and contact time were employed to ascertain the optimal condition for representative azo-dyes adsorption, including methyl orange (MO) and methylene blue (MB). The maximal adsorption of MO and MB on the CCGMs at pH values of 3 and 11 were 383.142 mg g$^{-1}$ and 584.795 mg g$^{-1}$, respectively. The adsorption mechanism were demonstrated as the synergistic effect of electrostatic interaction and $\pi$-$\pi$ stacking between dyes and CCGMs. Besides, the outstanding and stable regeneration of as-prepared CCGMs were also verified with five consecutive recycling. Thus, the newly developed CCGMs could be a highly promising candidate for dyestuff wastewater treatment.

**Keywords:** dyestuff wastewater treatment; amphoteric carboxymethyl chitosan/gelatin microspheres (CCGMs); pH induced selective removal; adsorption mechanism

## 1. Introduction

Printing and dyeing industry as one mainly source of wastewater, indiscriminate discharge of untreated dyestuff effluent with high concentration and toxicity has been threatening the ecological balance and human health [1-3]. Accidental intake of excessive dyes will cause irreversible harms, including serious headache, allergy and skin irritation, and even organ functional disorders because of their inherent toxic, mutagenic and carcinogenic features [4, 5]. Although numerous removal strategies including coagulation, chemical oxidation, membrane filtration, ion exchange and photocatalysis have been applied for dye-contaminated water purification, these techniques suffer from several shortcomings including limited operation condition, high investment costs, short lifetime and harmful by-products generation [5-9]. Therefore, the development of high-efficient dye-removal techniques for actual industrial applications has long been a challenge [10]. Especially, the presence of azo group and aromatic structure make the azo-dyes, represented by MO and MB, are difficult to eliminate by traditional chemical and biological degradation methods [11]. Thus, azo dyestuff wastewater treatment becomes increasingly urgent [1, 2]. Among those methods, adsorption is particularly regarded as an easy-operated, low-cost, recyclable and high-efficiency technologies [12-15].

To date, micro- and nano-scale polymers arouse intensive interest towards scientific researches especially in the adsorption field, due to its good physicochemical properties and controllable morphologies [16-18]. Especially, green adsorbents original from natural biomasses with particularly favorable advantages, such as biodegradability, biocompatibility, and renewability, are drawing more and more attentions for dyes contained wastewater treatment [19, 20]. Chitosan, as one of the most representative multi-functional polysaccharides, is an excellent chelating for heavy metals, radionuclides, dyes, *etc.*, due to its abundant and highly reactive 1,2-hydroxyl groups and amino groups [14, 21-27]. However, the further applications of chitosan are thwarted by its initial characteristics, including limited water-solubility and low acid resistance [28]. To make up for this deficiency, carboxymethyl chitosan (a potential chitosan derivative with superior water solubility), has been used as the precursor to build 3D structure. Additionally, the synergistic effect of carboxyl, hydroxyl and amino groups are helpful to further improve the binding ability towards adsorbate [29-31]. Nevertheless, heretofore, the reported maximum uptake capacity of carboxymethyl chitosan based adsorbents for MO and MB were 163 mg g$^{-1}$[32] and 349 mg g$^{-1}$[33], respectively, with large room for further improvements. Moreover, no work has been done so far to investigate the potential selective properties of amphoteric carboxymethyl chitosan based adsorbents, let alone reveals the selectivity mechanism and achieves superior and stable reusability.

To fulfill this research gap, in this study, novel CCGMs were developed by a facile inverse suspension method with two-step successive crosslinking process. Benefit from high activity and dispersion density of functional groups on carboxymethyl chitosan and gelatin molecules, high efficient pH induced selective adsorption and separation of azo-dyes can be easily realized. Considering the influential factors containing solution pH, temperature, and contact time, batch adsorption experiments were carried out to comprehensively evaluate the
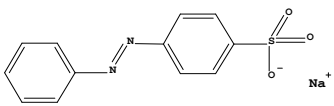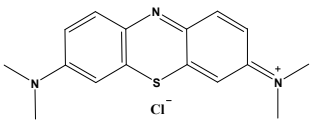
67 characteristics of CCGMs and systemically investigate the adsorption mechanism. As a result, the outstanding

68 structural and morphological capacities, as well as ultra-high adsorption properties of CCGMs were

69 demonstrated. The selective adsorption mechanism was proved to be the result of the synergistic effect of

70 electrostatic interaction and π-π stacking between dyes and CCGMs. Besides, CCGMs can also be regenerated

71 for further use through the desorption process with ionic exchange.

72

73 **2. Experiment**

74 2.1 Materials

75 Carboxymethyl chitosan (above 80% substitution degree) was purchased from Shanghai Source Biotechnology

76 Co., Ltd., Shanghai, China. Gelatin, n-octane, glutaraldehyde, acetone, and ethanol were purchased from Ling

77 Feng Chemical Co., Ltd., Shanghai, China. $CaCl_2$, NaCl, $NaNO_3$, $Na_2SO_4$ and $Na_3PO_4$ were provided by Titan

78 Chemical Technology, Co., Ltd. Span 80, MO, and MB were purchased from Reagent Co., Ltd., Shanghai,

79 China (more details see **Table 1**). All reagent (except n-octane) were analytical grade and used as received.

80 Distilled water was utilized in all of the experiments.

81 <center>**Table 1.** Characteristics of MB and MO.</center>

| Dye | Structural formula | Charge | Molecular formulae | $\lambda_{max}$ (nm) |
|-----|-------------------|--------|--------------------|-----------|
| MO |  | Anionic | $C_{14}H_{14}N_3NaO_3S$ | 464 |
| MB |  | Cationic | $C_{16}H_{18}ClN_3S \cdot 3H_2O$ | 668 |

82

83 2.2 Synthesis of CCGMs

84 CCGMs were prepared using an inverse suspension method with two-step successive crosslinking process

85 (**Fig.1**). Considering the solubility of gelatin components, the preparation of CCGMs was carried out at 60 °C

86 unless other stated. At first, carboxymethyl chitosan (0.5 g, 2 wt%) and gelatin (2.0 g, 8 wt%) were dissolved

87 by distilled water (25 mL) under continuous stirring on a thermostat water bath (HWCL-3, Zhengzhou

88 Greatwall Scientific Industrial and Trade Co., Ltd., Zhengzhou, China) over 20 h. The uniformly mixed

89 solution obtained from the above process serves as the dispersed phase. Second, the dispersed phase was

90 placed in a 20 mL syringe equipped with a flat nozzle (ø = 600 μm). Driven by a micro-syringe pump (LSP01-

91 1A, Longer Precision Pump Co., Ltd., Baoding, China), the dispersed solution was dropwise added into 100

92 mL 2 wt% $CaCl_2$ solution (The level difference between the $CaCl_2$ solution and the top of the nozzle was 15

<center>3</center>

cm.) at a speed of 60 mL h$^{-1}$. In this step, the dispersed solution leaving the flat nozzle formed into microspheres under the action of their own gravity and interfacial tension. Then, the microspheres started the physical crosslinking process at the moment of passing through the air-liquid interface of CaCl$_2$ solution. After gentle stirring (300 rpm) for 30 min, the coagulated microspheres were washed several times with excess distilled water before being transferred into 100 mL 1 wt% glutaraldehyde solution for chemical crosslinking procedure. The chemical crosslinking process was performed at the same condition as previous physical one. Finally, as-prepared CCGMs were thoroughly washed with acetone, ethanol and distilled water successively before the final drying at 40 °C for 8 h in an oven (DHG- 9023A, Shanghai Jingruo Scientific Instrument Co., Ltd., Shanghai, China).



**Fig.1** (a) The overview of the synthesis process of CCGMs; (b) Batch adsorption experiments for MO and MB.

2.3 Characteristics of CCGMs

Characterizations of CCGMs were systematically analyzed by Fourier transform infrared spectroscopy (FT-IR, Nicolet 6700, Thermo Fisher, America), scanning electron microscope (SEM, NOVA Nano SEM 450, FEI, America), and X-ray photoelectron spectroscopy (XPS, Thermo Fisher Scientific, America). Thermal analysis

4

109 of CCGMs was accomplished on a Thermo Gravimetric Analyzer (Pyris 1 TGA, PerkinElmer Co., Ltd,

110 America) in the temperature range of 40–800 °C with a heating rate of 10 °C min$^{-1}$ in a nitrogen medium. The

111 parameters of the above analytical instruments can be found in the Supporting Information (SI).

112 The morphology investigation of CCGMs was carried out employing an optical microscope (AZ100, Nikon,

113 Japan). Particle monodispersity was defined using coefficient variation (CV), which can be calculated as:

114
$$CV = \frac{\sqrt{\left(\sum_{i=1}^{N} \frac{(D_i - \overline{D_n})^2}{(N-1)}\right)}}{\overline{D_n}} \times 100\% \tag{Eq.1}$$

115 where $D_i$ (μm) and $\overline{D_n}$ (μm) are the diameter and the average diameter of CCGMs, respectively. $N$ is the

116 sample size, which was 200 in this study. In addition, the BET surface area was calculated from the adsorption

117 branches in the relative pressure range of 0.1-0.3.

118

119 2.4 Batch adsorption experiment

120 1000 mg L$^{-1}$ MO and MB stock solution were firstly prepared by dissolving the corresponding azo-dye powder

121 into a certain distilled water, respectively, and then diluted to a certain concentration from 50 mg L$^{-1}$ to 300 mg

122 L$^{-1}$. The adsorption experiment was carried out by adding a certain amount of CCGMs to a 50 mL centrifuge

123 tube containing a specified concentration of dye-solution. The centrifuge tube was placed under a constant

124 thermal oscillated condition (60 °C, 250 rpm) to reach adsorption equilibrium (about 4 h). The initial pH of

125 dye-solution was adjusted by 0.1 M HCl and 0.1 M NaOH solution, and measured by a pH meter (3110-SET2,

126 WTW, Germany). The MO and MB concentration were measured using an UV spectrophotometer (UV-1800,

127 Shimadzu, Japan) with the peaks of the absorbance ($\lambda_{max}$) at 464 and 668 nm, respectively. Besides, the

128 calibration curves were measured at different pH conditions (pH=3, 5, 7, 9, 11) and used separately to avoid

129 any potential influence from different pH values.

130 The adsorption experiments were performed in duplicate. The initial concentration of the MO and MB were set

131 as 200 mg L$^{-1}$ for the kinetic adsorption experiments. Additionally, the initial pH of dye-solution were 3 for

132 MO and 11 for MB, respectively. Adsorption isotherm and thermodynamic analysis were also investigated

133 through altering the initial concentration of dye-solution and adsorption temperature. Adsorption capacity was

134 determined with the equations as following:

135
$$q_t = \frac{(C_0 - C_t)V}{m} \tag{Eq.2}$$

136
$$q_e = \frac{(C_0 - C_e)V}{m} \tag{Eq.3}$$

137 Where $C_0$ (mg L$^{-1}$) and $C_t$ (mg L$^{-1}$) are initial and instant concentration (at a predetermined time $t$) of MO or

138 MB in the dye-solution, respectively. $C_e$ is the equilibrium concentration of MO or MB. $V$ is the volume of

139     solution. *m* is the weight of CCGMs used in the experiments.

140     Besides, for the study of selective adsorption, the experiment was performed by using the binary mixture (20

141     mg $L^{-1}$ for MO and 20 mg $L^{-1}$ for MB) at different pH conditions. The concentration change of targeted dyes in

142     the filtered supernatant at different time was monitored and measured with an UV-spectrometer.

143

144     2.5 Desorption experiment

145     In order to realize the recycle and regeneration of CCGMs, a pH-induced desorption experiment was

146     conducted in duplicate. The initial and residual dye concentrations were measured following the same method

147     in the adsorption experiments.

148

149     **3. Results and Discussion**

150     3.1 CCGMs Characterization

151     The SEM images of the surface and cross-section of a single CCGM are shown in **Fig.2**. The CCGM exhibited

152     quasi-spherical state with rough surface (**Fig.2a and b**, the average specific surface area of as-prepared

153     CCGMs tested by BET method was 18.73 $m^2$ $g^{-1}$), which was beneficial for dyes adsorption. The average

154     diameter of CCGMs was around 1060 μm. Besides, the relatively narrow size distribution (CV= 8.6%) was

155     also demonstrated. The SEM images of the cross-section show randomly distributed hierarchical pores with a

156     pore size of 10 to 35 nm (**Fig.2c and d**), which greatly facilitate the diffusion and adsorption of dye molecules

157     from the surface to the interior of CCGMs. More importantly, the apparent porous structure changes and the

158     transition zone in the cross-section displayed in **Fig.2d** can be attributed to the sequential physical and

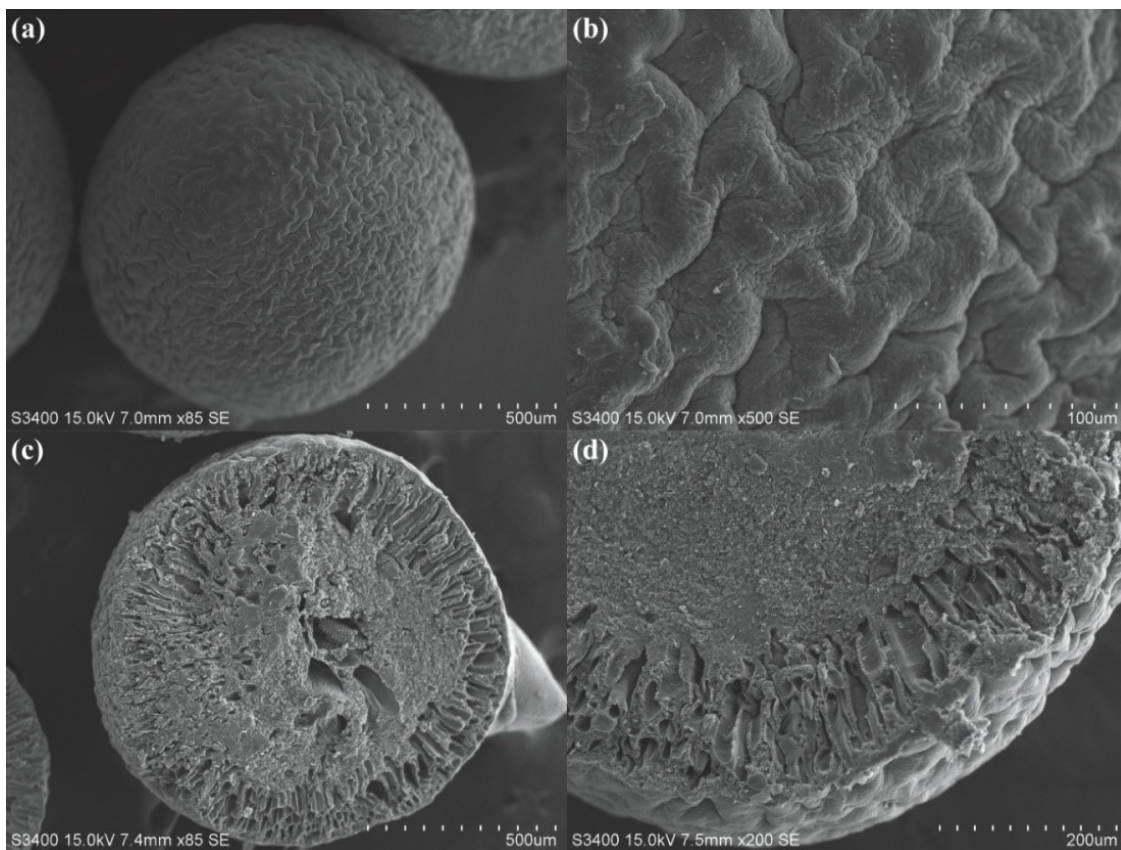159     chemical crosslinking processes.

**Fig.2** SEM images of (a) a single CCGM; (b) local surface amplification of CCGM; (c) inner structure of CCGM; (d) local amplification of a cross section of the CCGM.

The FT-IR spectra of the carboxymethyl chitosan powder, gelatin powder, CCGMs, MO adsorbed CCGMs and MB adsorbed CCGMs are compared in **Fig.3** in order to monitor the characteristic functional groups changes, and identify the key functional groups of CCGMs responsible for the binding of different azo-dyes. The basic characteristic peaks of carboxymethyl chitosan were found at approximately 3425 cm$^{-1}$ (N-H and O-H stretching vibrations), 2920 cm$^{-1}$ and 2881 cm$^{-1}$ (C-H symmetric and asymmetric stretching vibration), 1606 cm$^{-1}$ (the N-H bending vibrations), 1419 cm$^{-1}$ (the symmetric stretching vibrations of COO- groups), and 1078 cm$^{-1}$ (C-O stretching vibrations) [31, 34]. Gelatin was characterized as its C=O stretching of amide (I) peak at 1635 cm$^{-1}$ and N-H bending vibration of amide (III) at 1181 cm$^{-1}$ [35]. However, in the cross-linked CCGMs, the symmetric (1419 cm$^{-1}$) stretching vibration of the COO- groups was shifted to 1410 cm$^{-1}$, due to the ionic interaction between the carboxylic groups and the calcium ions during the first physical crosslinking step. Besides, comparing to the spectrum of carboxymethyl chitosan, a new peak at around 1653 cm$^{-1}$ appeared, which can be attributed to the C=N linkage derived from the Schiff's base. It clearly demonstrated that the second chemical crosslinking reaction between aldehyde groups of glutaraldehyde and the amino groups of carboxymethyl chitosan and gelatin was successful.

7

178 Moreover, as shown in the spectra of MB-CCGMs (**Fig.3**), the corresponding peak of the symmetric (1419 cm-
179 $^1$) stretching vibrations of the COO- groups of CCGMs was further shifted to 1390 cm$^{-1}$. At the same time, the
180 characteristic peak of N-H bending vibrations (1581 cm$^{-1}$) of CCGMs was also changed to 1545 cm$^{-1}$,
181 indicating that carboxyl and amino groups of CCGMs participated in MB adsorption. However, for MO uptake,
182 the characteristic peak of N-H bending vibrations at around 1581 cm$^{-1}$ of CCGMs was shifted to 1560 cm$^{-1}$,
183 while the peak of the COO- groups of CCGMs at around 1410 cm$^{-1}$ was almost unchanged after adsorption
184 equilibrium. Thus, it indicates that the MO adsorption process is dominated by amino groups of CCGMs.
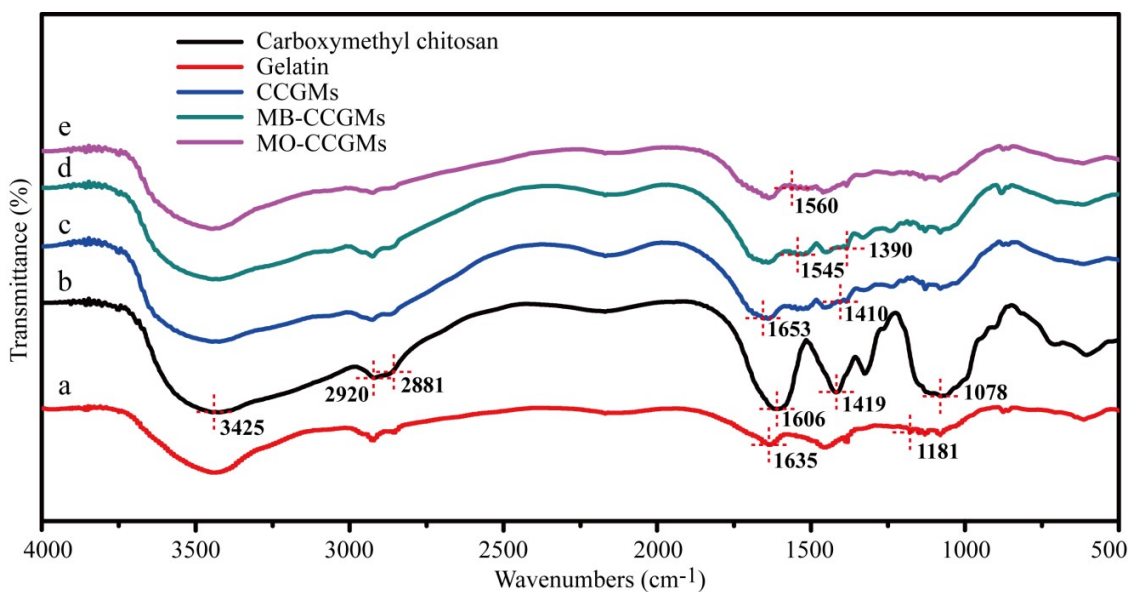


186 **Fig.3** The FT-IR spectrums of (a) gelatin, (b) carboxymethyl chitosan, (c) CCGMs, (d) MB-CCGMs and (e)
187 MO-CCGMs, respectively.

188

189 X-ray photoelectron spectroscopy (XPS) analysis, as an effective method, is of great value for the investigation
190 of elemental composition of materials and electronic interaction at the interface [16]. As shown in **Fig.4a**, the
191 C1s XPS spectrum of the CCGMs shows three characteristic peaks corresponding to C-C and C-H bonds
192 (284.55 eV), C-O-bond (285.1 eV) and –O-C=O bond (286.1 eV), respectively [36]. Comparing with CCGMs,
193 after the adsorption of MO (**Fig.4b**) and MB (**Fig.4c**), the binding energy of C-O- increased from 285.1 eV to
194 285.7 eV and 286.15 eV, respectively, while, the binding energy of –O-C=O increased from 286.1 eV to
195 286.55 eV and 287.9 eV, respectively. It's worthy mentioned that the characteristic peak of π-π appeared at
196 288.0 eV was shifted to 288.2 eV (MO, **Fig.4b**) and 289.0 eV (MB, **Fig.4c**), which can be attributed to
197 hydrogen bond, indicating that electrostatic interactions and π-π stacking contribute to the dyes-CCGMs
198 binding. **Fig.4d-f** show the O1s spectra of CCGMs before and after the adsorption of MO and MB. The most
199 intense peaks of CCGMs are assigned to C-O, O-H or bound H$_2$O (532.8 eV), C=O or C-O-C (531.65 eV) and
200 O-metal (530.8 eV), respectively [37]. After adsorbing MO and MB, the peak located at 532.8 eV increased to

533.25 eV and 533.2 eV, respectively, while, the peak of C=O or C-O-C located at 531.65 eV shifted to 532.35 eV and 532.1 eV. Evidently, such results originate from the fact that oxygen atom provides electron pairs for MB and MO adsorption. This further indicates that electrostatic interactions are involved in the dyes-CCGMs adsorption process [33]. High resolution XPS spectra of N 1s of the sorbent before and after MO and MB uptake are compared in **Fig.4g-i**. The peak at the position of 399.25 eV is assigned to -NH$_2$ or -NH- groups, whereas the peak at 399.85 eV is due to C=N-C or O=C-N groups. Additionally, the N 1s spectrum of the CCGMs at the blinding energy of 400.4 eV is attributed to C-N-C or C-NH$_3^+$ groups [38, 39]. After MO and MB adsorption on CCGMs, the mentioned blinding energy of 399.25 eV increased to 399.65 eV and 399.45 eV, respectively, while, the blinding energy of 400.4 eV shifted to 400.7 eV and 400.55 eV. However, the blinding energy of 399.85 eV for C=N-C or O=C-N groups was almost unchanged. All above implies that -OH, -COOH, and -NH$_2$ groups are involved in the adsorption process and the synergistic effect of electrostatic interaction and π-π stacking between dyes and CCGMs are the main driving force for dyes-adsorbent adsorption process [16].
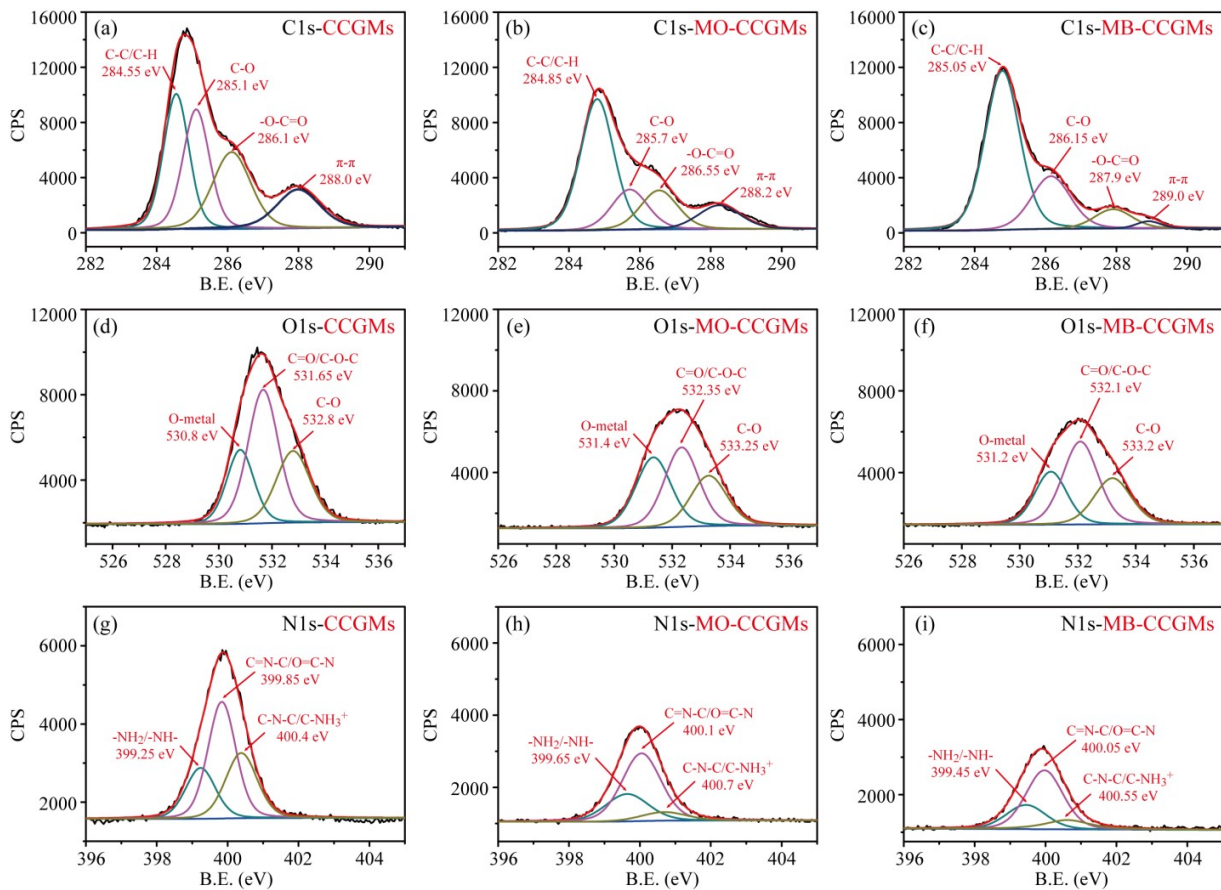


**Fig.4** C1s XPS spectra of (a) CCGMs, (b) MO-CCGMs, and (c) MB-CCGMs; O1s XPS spectra of (d) CCGMs, (e) MO-CCGMs, and (f) MB-CCGMs; N1s XPS spectra of (g) CCGMs, (h) MO-CCGMs, and (i) MB-CCGMs.

217  Thermo gravimetric weight charge curves of the obtained samples, including CCGMs, MO-CCGMs, and MB-
218  CCGMs, are compared in **Fig.5**. As shown in **Fig.5**, all three samples followed similar three-stage weight loss
219  trend upon heating in nitrogen. The initial weight loss of 13.23% (**Fig.5b**) in the range of 40 - 230 °C, is due to
220  the removal of physically adsorbed solvent and surface hydroxyl groups [30]. However, less weight loss are
221  observed from the TGA curves of MO- and MB-CCGMs (**Fig.5c and d**), which can be attributed to its re-
222  drying process with low temperature after dyes adsorption equilibrium. The decomposition and ablation of
223  carboxymethyl chitosan and gelatin molecule chains start at around 230 °C with high percents of weight loss
224  (60.74% for CCGMs, 55.12% for MO-CCGMs, and 58.84% for MB-CCGMs). As the heating temperature
225  continues to rise, reaching 800 °C, the samples degradation enters the final stage, where the weight loss of
226  samples can be attributed to the molecular carbonization of carboxymethyl chitosan, gelatin (and azo-dyes).
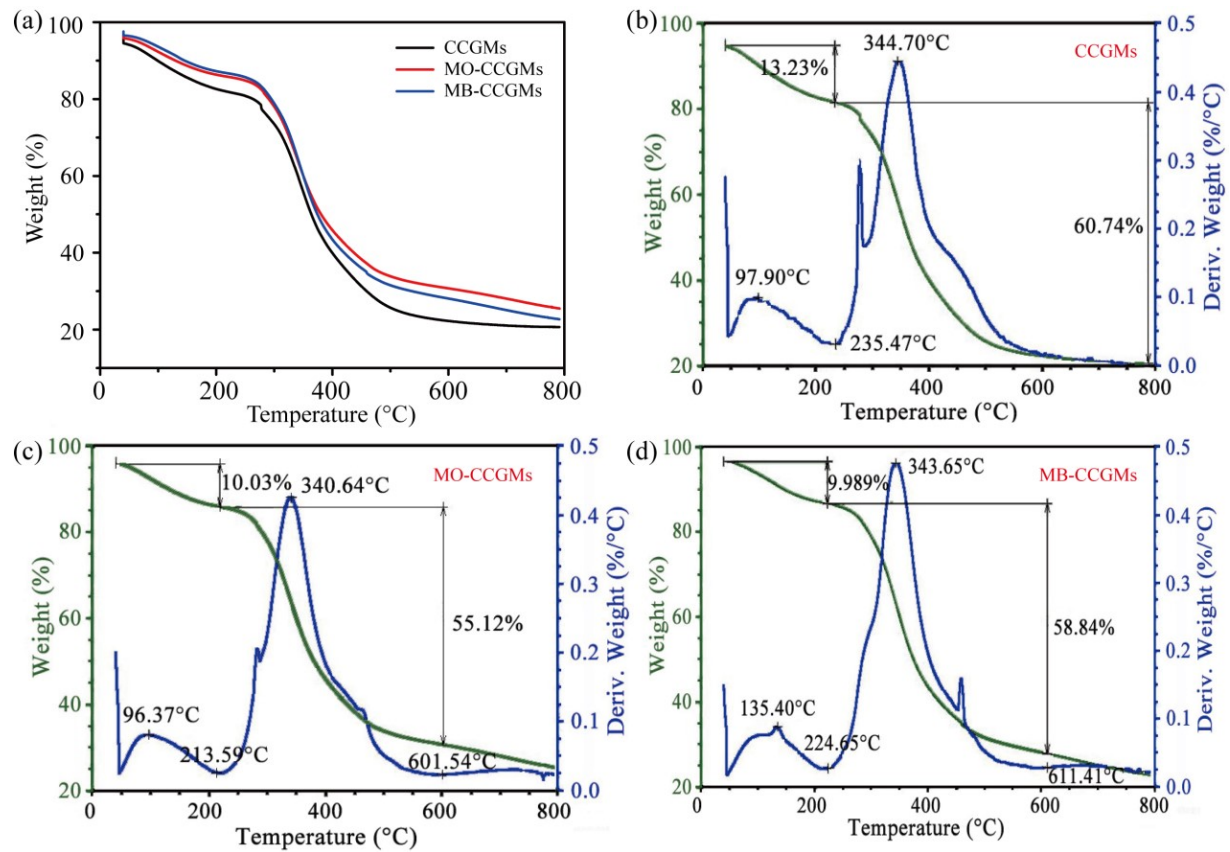


228  **Fig.5** (a) Thermo gravimetric analysis of CCGMs, MO-CCGMs and MB-CCGMs; TGA curves of (b) CCGMs,
229                              (c) MO-CCGMs and (d) MB-CCGMs.

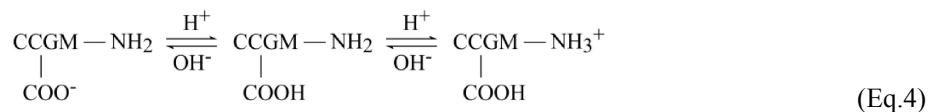230

231  3.2 Selective adsorption studies

232  3.2.1 pH effect

233  Point of zero charge ($pH_{pzc}$), which represents the pH value of adsorbent when the charge on its surface is zero,

234  plays a key role in the surface science of environmental interfaces. In this paper, the $pH_{pzc}$ of as-prepared

235  CCGMs were measured via drift method [40]. More specifically, the initial pH of 50 mL of 0.01 M NaCl

236  solution was adjusted to pH ranging from 3-12 by adding either 0.1 M HCl or 0.1 M NaOH solution. 0.2 g of

237  CCGMs were added and gently stirred for 48 h at 300 rpm. The $pH_{pzc}$ was noted at the pH where the final pH

238  ($pH_{final}$) was equal to the initial pH ($pH_{initial}$). At solution pH below $pH_{pzc}$, the surface of CCGMs is positively

239  charged, which will show good affinity to anionic dyes, that is, MO in this study. Vice versa, at pH above the

240  $pH_{pzc}$, the surface becomes negatively charged, which is favorable for cationic dyes (MB) binding via

241  electrostatic interaction between cations and CCGMs.

242  As shown in **Fig.6a**, the $pH_{pzc}$ of as-prepared CCGMs was 6.68. Simultaneously, as shown in **Fig.6b**, the

243  adsorption of the MO was decreased, while that of the MB was increased with an increase in the initial pH

244  levels. The highest uptake of MO and MB was observed at pH levels of 3 and 11, respectively. At pH levels of

245  4 and above, $-NH_2$ groups on CCGMs is not fully protonated due to insufficient protons ($H^+$) and still kept as -

246  $NH_2$. As a result, it is difficult for MO molecules to interact with CCGMs, giving rise to low adsorption

247  capacities. While, with the pH increasing, more $COO^-$ groups on CCGMs will attract more monovalent

248  quaternary ammonium cationic groups of MB by electrostatic interactions. Similarly, at pH levels of 9 and

249  below, the adsorption of CCGMs towards MB decreased. This results may be attributed to the electrostatic

250  repulsion between the $-NH_3^+$ groups of the CCGMs and the cationic MB.

251  The adsorption mechanism of CCGMs for MO and MB is demonstrated as electrostatic and π-π stacking

252  interactions with the active functional groups of CCGMs, such as amino, hydroxyl as well as carboxyl groups.

253  Among them, amino groups play a dominant role in the impacts of adsorption ability of CCGMs. Especially, in

254  the acid condition, positively-charged amino groups ($NH_3^+$) have strong electrostatic affinity with $SO_3^-$ groups

255  on MO. The negative charge density of the CCGMs increased with the association of $OH^-$ ions onto their

256  surfaces in an alkaline condition, the -COOH groups were also deprotonated and formed into $-COO^-$ groups at

257  high pH levels. Thus, the pH effect of adsorption properties of CCGMs for two dyes with very different

258  electrical properties can be summarized as the following balance (Eq.4):

$$CCGM-\underset{\underset{COO^-}{|}}{NH_2} \overset{H^+}{\underset{OH^-}{\rightleftharpoons}} CCGM-\underset{\underset{COOH}{|}}{NH_2} \overset{H^+}{\underset{OH^-}{\rightleftharpoons}} CCGM-\underset{\underset{COOH}{|}}{NH_3^+}$$

259  (Eq.4)

260  The above balance will move toward the right at the dye solution pH decreasing. Thus, more $NH_3^+$ groups on

261  CCGMs will be obtained and attract more $SO_3^-$ groups of MO by electrostatic interactions.
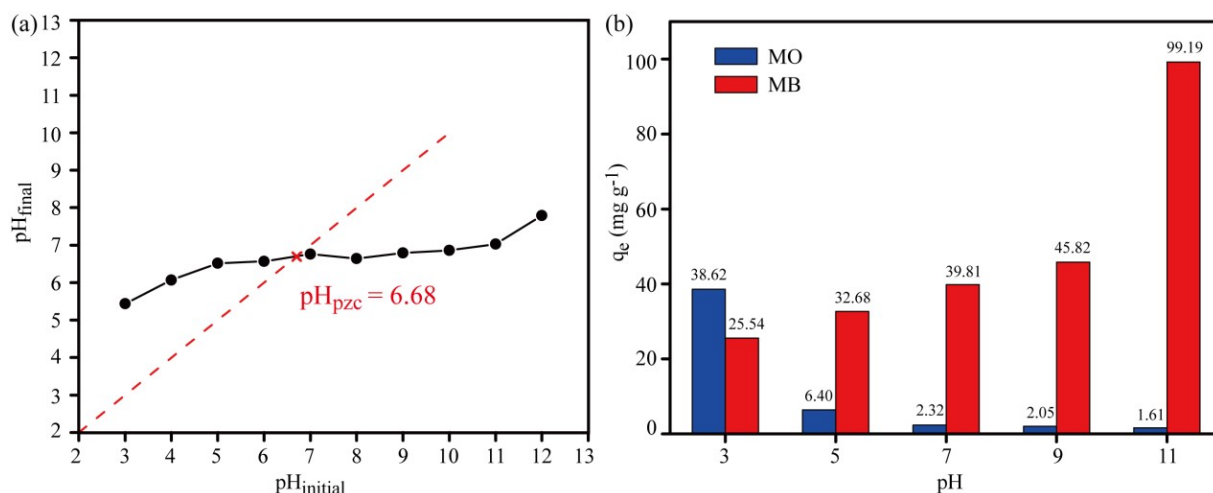
**Fig.6** (a) pH$_{pzc}$ of CCGMs by drift method; (b) The effect of initial pH on adsorption performance of CCGMs towards MO and MB.

### 3.2.2 Inorganic anions effect

Generally, in the textile industries, multiple electrolytes are added to the dyeing bath to improve dyeing fastness at the expense of dyeing rate [41]. Furthermore, it has been reported that the addition of sodium chloride or sodium sulfate can properly maintain or protect the strength of silk or woolen fibers in the acidic dying [42]. Therefore, the existence of inorganic anions, such as chloride (Cl$^-$), nitrate (NO$_3^-$), sulfate (SO$_4^{2-}$), and phosphate (PO$_4^{3-}$), is considerably common in practical textile industry effluents. However, the effect of competing inorganic anions on the adsorption performance of MO dyes onto CCGMs, dominated by electrostatic attraction, cannot be ignored.

Herein, a different sodium salt (0.01 M) was added each time to 20 mg L$^{-1}$ MO solution and 200 rpm agitation speed. As expected, the present of inorganic salts significantly hindered the adsorption of MO dyes onto the CCGMs, as seen in **Fig.7a**. The order of inhibition capacity was PO$_4^{3-}$ > SO$_4^{2-}$ > NO$_3^-$ > Cl$^-$, which was consistence with the conclusion of previous study [43]. This phenomenon can be attributed to the fact that the trivalent electrolyte Na$_3$PO$_4$ had the most negative charges among all the other bivalent and univalent electrolytes and displayed the strongest competition toward adsorption sites.

Besides, the effect of the concentration of inorganic anions represented by Cl$^-$ on MO adsorption was further studied by changing the amount of added sodium chloride. As shown in **Fig.7b**, with the increase of sodium chloride, the adsorption property of as-prepared CCGMs for anionic MO dyes slightly decreased. The reason for this phenomenon is that the dielectric constant of the solution decreases with the increase of ionic strength. It can be speculated that under strong acidic conditions, the proton amino groups in CCGMs has stronger binding energy with anionic MO molecule, thereby inorganic anions have less influence on the adsorption
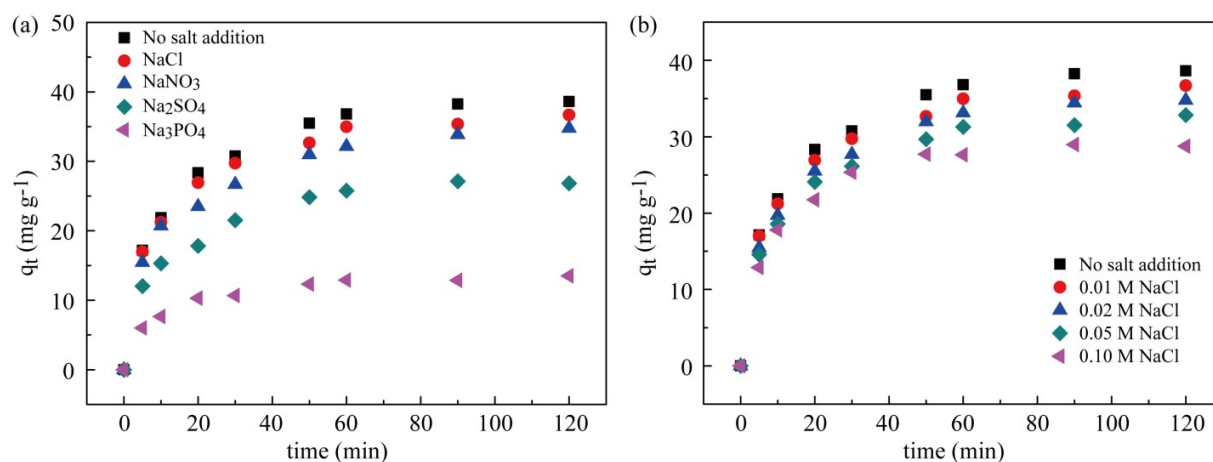
12

Fig.7 Effect of (a) type and (b) concentration of inorganic anions on MO adsorption of CCGMs.

### 3.2.3 pH-induced selectivity

As the selective adsorption of targeted dyes has practical significance, the separation ability of as-prepared CCGMs towards dyes mixture was also been investigated. In this paper, as shown in **Fig.S1** and **Fig.S2**, the irrelevancy of characteristic peaks of different dyes in binary UV spectra was verified by varying pH conditions (pH=3 and 11) and mass fraction ratios of MO to MB (9:1, 7:3, 5:5, 3:7 and 1:9). In this regard, to exclude the influence of dye concentration difference, the selective adsorption of MO and MB onto CCGMs were performed using the binary mixture with a mass ratio of 5:5 (20 mg $L^{-1}$ for MO and 20 mg $L^{-1}$ for MB) at initial pH levels of 3 and 11, respectively. The filtered supernatant of binary mixture was monitored with an UV spectrometer during the selective adsorption process with continuously stirring at 300 rpm for 5 h.

As shown in **Fig.8d**, the color of the binary mixture changed from original dark green to light green under acidic condition (pH =3) due to the MO incomplete removal. This result was also verified by the characteristic peaks changes. As exhibited in **Fig.8a**, the characteristic peak of MO decreased drastically but did not disappear in the end. While, the characteristic peak of MB only show a slight decrease in this process. Oppositely, in the alkaline environment (pH=11, **Fig.8e**), compared with individual dye adsorption, the color of the binary mixture changed from initial dark green to bright yellow, which is the pure MO color. It suggested that the cationic dye MB was adsorbed preferentially and thoroughly by CCGMs, and only anionic dye MO is remained in the mixture solution. Consistent result was observed by the UV spectra showing in **Fig.8b**. Therefore, pH-induced selectivity of CCGMs for MO and MB is demonstrated as the result of the electrostatic attraction between CCGMs and dyes.
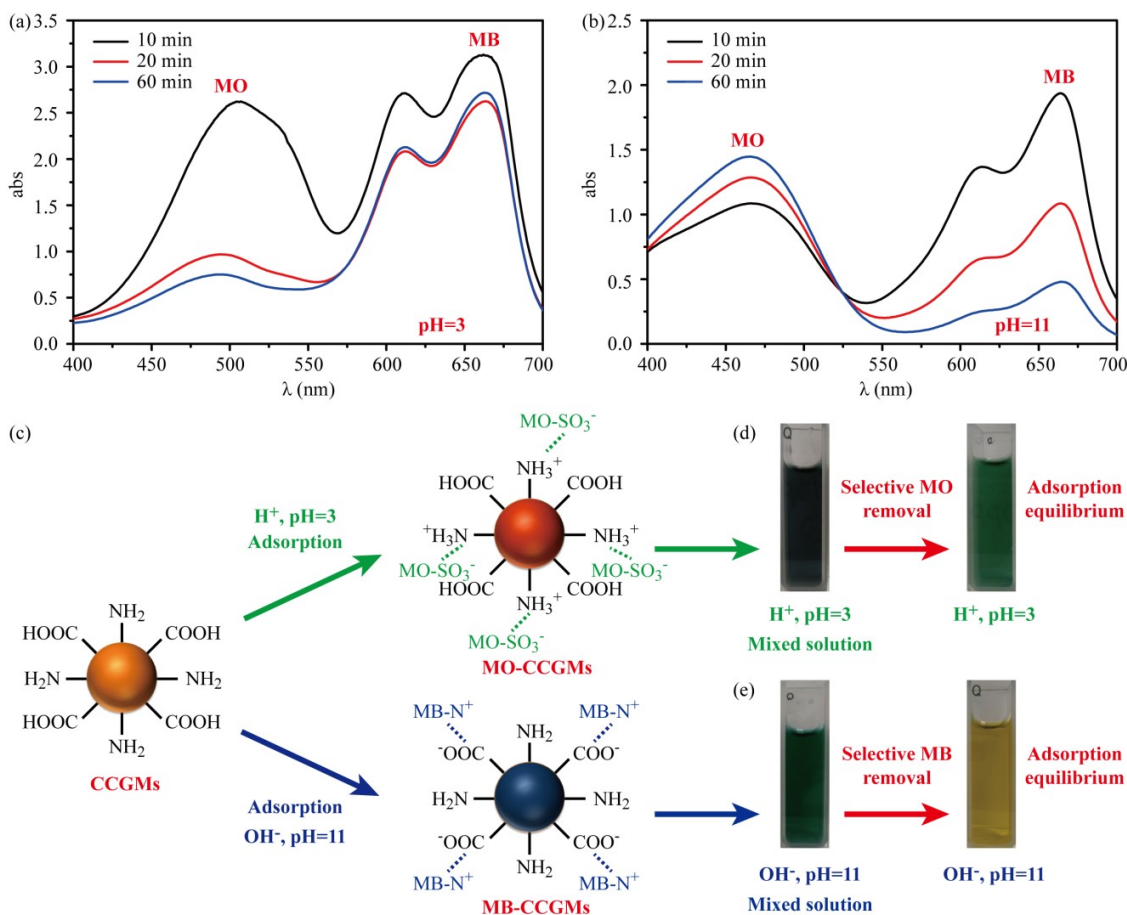
13

**Fig.8** The UV-spectra of the MO and MB mixed solution at (a) pH = 3 and (b) pH = 11, respectively; (c) pH-induced selective adsorption mechanism; (d) Digital images of the color change of the binary mixture at (d) pH = 3 and (e) pH = 11, respectively.

3.3 Desorption and regeneration

In order to realize the reusability of the CCGMs, inverse pH-induced desorption process was performed for several adsorption-desorption cycles. Under alkaline condition (pH=11), amino groups on the CCGMs are kept in the form of -NH$_2$, which is quite difficult to adsorb negative MO. Thus, the desorption behavior is mainly attributed to the electrostatic repulsion between sulfo (SO$_3^-$) groups on MO molecules and the negatively charged carboxyl groups (COO$^-$) on CCGMs (see **Fig.9a**). Similarly, MB desorption and CCGMs regeneration can be achieved under acidic condition (pH=3). In this case, carboxyl group on CCGMs are kept in the form of -COOH, the desorption behavior is mainly attributed to the electrostatic repulsion between N$^+$ groups on MB and the positively charged amino groups (NH$_3^+$) on CCGMs (see **Fig.9a**). The adsorption and desorption efficiency of MO and MB at each recycling cycle are shown in **Fig.9b**. The desorption efficiency of MO and MB were maintained above 90% and the adsorption of the MO and MB maintained above 80% after 5 cycles.

14

325  The results indicated that as-prepared CCGMs could be used repeatedly in the MO and MB adsorption

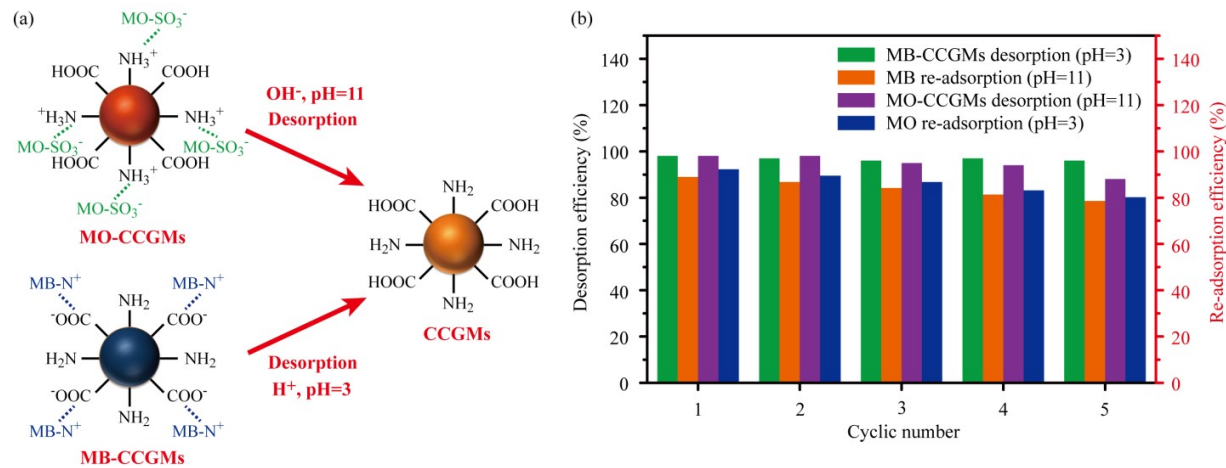326  experiment with a small adsorption capability loss.



328  **Fig.9** (a) Schematic illustration of the inverse pH-induced desorption process; (b) Desorption and re-adsorption

329  efficiency of as-prepared CCGMs for MO and MB, respectively.

330

331  3.4 Kinetic studies

332  Kinetics models are generally employed to correlate adsorption rates and equilibrium time. In order to

333  investigate the adsorption behaviors of two representative azo-dyes, herein, pseudo-first order model, pseudo-

334  second order and intraparticle diffusion model were employed at different pH conditions (pH=3 for MO while

335  pH=11 for MB).

336

337  3.4.1 Pseudo-first and -second order model

338  Pseudo-first order and pseudo-second order kinetic models are normally expressed using the following

339  equations:

340
$$log\,(q_e - q_t) = logq_e - \frac{k_1}{2.303}t \qquad \text{(Eq.5)}$$

341
$$\frac{t}{q_t} = \frac{1}{k_2 q_e^2} + \frac{1}{q_e}t \qquad \text{(Eq.6)}$$

342  Where $q_e$ (mg g$^{-1}$) and $q_t$ (mg g$^{-1}$) are the amounts of adsorbed MO and MB at equilibrium and at time $t$ (min),

343  respectively; $k_1$ (mg g$^{-1}$ min$^{-1}$) and $k_2$ (mg g$^{-1}$ min$^{-1}$) are the corresponding rate constants for pseudo-first and -

344  second order model, respectively.

345  As illustrated in **Fig.10a**, the highly efficient adsorption characteristics of as-prepared CCGMs for MO and

346  MB has been demonstrated. In particular, for MO adsorption process, the equilibrium time was less than 60

min, which was almost half of the saturated uptake time for MB. The early-time large adsorption rate for both dye targets observed from the adsorption kinetic curves (**Fig.10a**) can be attributed to the large specific surface area and abundant binding sites on the surface of CCGMs. Besides, compared with pseudo-first order model (**Fig.10b**), the kinetics fitting curves of pseudo-second model for MO and MB adsorption (**Fig.10c**) show better linear characteristics since the correlation coefficient ($R^2$) of both are closer to 1, up to 0.996 and 0.995 for MO and MB, respectively. All kinetic parameters derived from the pseudo-first order model and the pseudo-second order model are summarized in **Table 2**. Additionally, it was confirmed simultaneously that as-prepared CCGMs exhibited stronger affinity to the cationic dye, MB, under alkaline condition, than the anionic one, MO, under opposite pH condition, which can ascribe to stronger electrostatic attraction between MB and CCGMs [16, 30].

3.4.2 Intraparticle diffusion model

Apart from the above two models, more adsorption process details can be further understood by introducing the intraparticle diffusion model. The most commonly format for intraparticle diffusion model can be expressed as [44]:

$$q_t = k_i t^{0.5} + I \tag{Eq.7}$$

where $k_i$ (mg g$^{-1}$ min$^{-0.5}$) is the rate constant of intraparticle diffusion model and the intercept $I$ is related to the boundary layer thickness.

As shown in **Fig.10d**, nearly linear variations reflected from the kinetics curves indicate that the whole adsorption process is companioned with physical diffusion effect. However, the correlation coefficient ($R^2$) of linear fitting curves for intraparticle diffusion model were merely 0.972 and 0.944 for MO and MB adsorption, which are smaller than those obtained from pseudo-second order model fittings (more than 0.995), indicating that chemisorption is dominated in the whole process. Meanwhile, it has also proven that the dye removal rate is depended and controlled by electrostatic interaction [45].

**Table 2.** Kinetic models fitting of MB and MO on CCGMs.

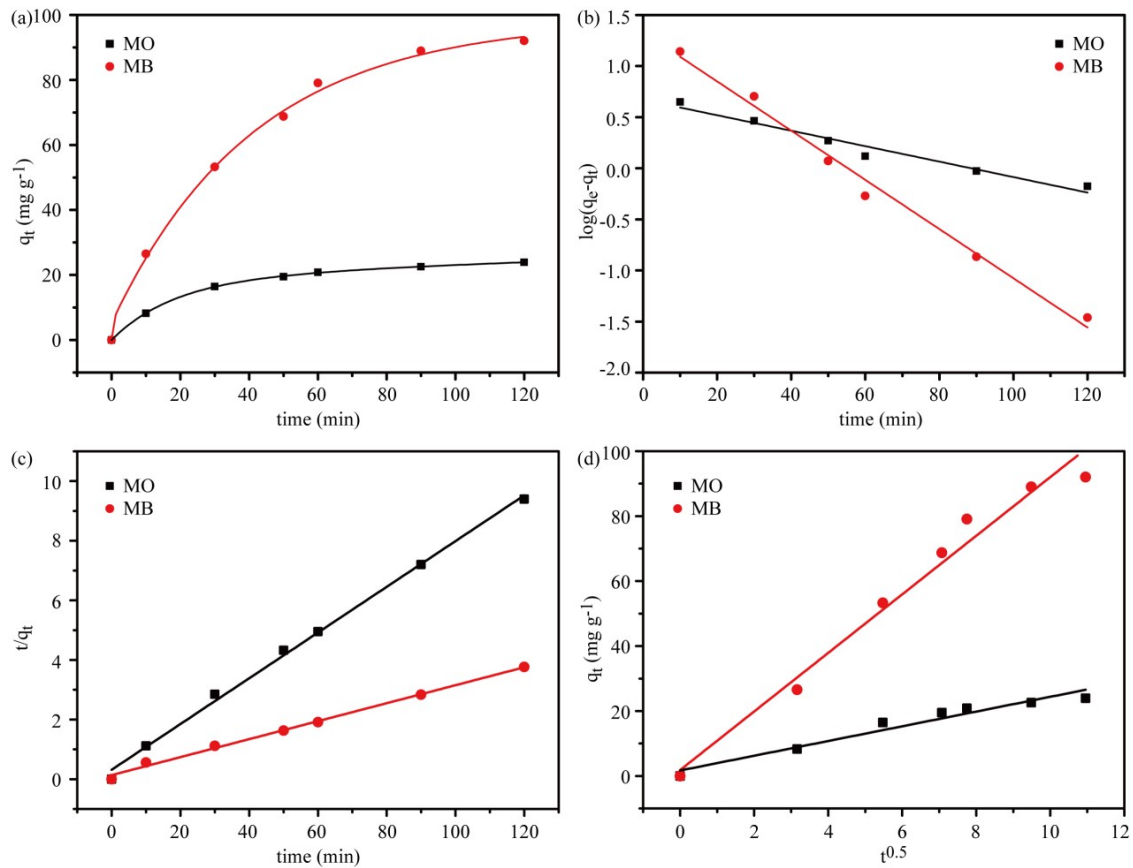| Kinetic models | MO (pH=3) Parameters | | | MB (pH=11) Parameters | | |
|---|---|---|---|---|---|---|
| **Pseudo-first order model** | $q_{e,cal}$ (mg g$^{-1}$) | $k_1$ (mg g$^{-1}$ min$^{-1}$) | $R^2$ | $q_{e,cal}$ (mg g$^{-1}$) | $k_1$ (mg g$^{-1}$ min$^{-1}$) | $R^2$ |
| | 4.683 | 0.017 | 0.954 | 21.458 | 0.055 | 0.987 |
| **Pseudo-second order model** | $q_{e,cal}$ (mg g$^{-1}$) | $k_2$ (mg g$^{-1}$ min$^{-1}$) | $R^2$ | $q_{e,cal}$ (mg g$^{-1}$) | $k_2$ (mg g$^{-1}$ min$^{-1}$) | $R^2$ |
| | 13.028 | 0.019 | 0.996 | 33.146 | 6.738E-3 | 0.995 |
| **Intraparticle diffusion model** | $I$ (mg g$^{-1}$) | $k_i$ (mg g$^{-1}$ min$^{-0.5}$) | $R^2$ | $I$ (mg g$^{-1}$) | $k_i$ (mg g$^{-1}$ min$^{-0.5}$) | $R^2$ |
| | 1.814 | 9.019 | 0.972 | 1.700 | 2.268 | 0.944 |

16

372



373

374    **Fig.10** (a) The typical adsorption kinetics; The fitting curves of (b) pseudo-first order model, (c) pseudo-
375               second-order model, and (d) intraparticle diffusion model.

376

377   3.5 Adsorption isotherm analysis

378   To better understand the adsorption behavior of CCGMs for two type azo-dyes, herein, the following
379   adsorption isotherm models were considered: Langmuir model, Freundlich model and Dubinin-Radushkevich
380   (D-R) model. The adsorption processes were performed at pH=3, 30 °C for MO, and pH=11, 60 °C for MB,
381   respectively, considering different adsorption properties of the two selected dyes. The corresponding
382   parameters are summarized in **Table 3**.

383

384   3.5.1 Langmuir model

385   The Langmuir equation is valid for monolayer sorption onto a surface with a finite number of binding sites.
386   Once the binding sites are occupied, they cannot interact with other adsorbates [46]. In general, the Langmuir
387   model can be expressed as follows:

17

$$\frac{C_e}{q_e} = \frac{1}{K_L q_m} + \frac{C_e}{q_m} \qquad \text{(Eq.8)}$$

Where $C_e$ (mg L$^{-1}$) is the equilibrium concentration of MO and MB; $q_e$ (mg g$^{-1}$) is the adsorption capacity at equilibrium; $q_m$ (mg g$^{-1}$) is the maximum adsorption capacity; $K_L$ (L mg$^{-1}$) is Langmuir constant.

As shown in **Fig.11a**, the adsorption isotherm curves were well fitted with Langmuir equation. The calculated maximum adsorbance of CCGMs were 383.142 mg g$^{-1}$ and 584.795 mg g$^{-1}$, respectively, close to the experiment results. The correlation coefficient ($R^2$) obtained from MO and MB uptake are more than 0.99, reach 0.995 and 0.998, respectively. The good fits in the Langmuir model **(Fig.11a)** indicate that predominantly active sites on the adsorbents surface are homogeneous distribution, which is beneficial for dye molecules forming uniform adsorption monolayer on the surface of the CCGMs.

3.5.2 Freundlich model

The empirical Freundlich equation is based on heterogeneous sorption system [47]. The linear Freundlich adsorption equation can be represented as:

$$log q_e = log K_F + \frac{1}{b} log C_e \qquad \text{(Eq.9)}$$

Where $C_e$ is the equilibrium concentration of MO and MB; $q_e$ is the adsorption capacity at equilibrium; $K_F$ and $b$ are Freundlich constants. The magnitude of Freundlich constant $b$ gives an indication on the favorability of adsorption and $K_F$ is regarded as the adsorption capacity when $C_e$ is unit concentration.

As shown in **Fig.11b**, the Freundlich model generated an acceptable fit to the experimental data ($R^2$ is 0.988 for MO and 0.986 for MB, respectively). However, the Langmuir isotherm shows a better fit to the adsorption data with larger $R^2$ than the Freundlich isotherm in the sorption of the two dyes. Additionally, the obtained value of Freundlich constant, $b$, indicates moderately favorable adsorption, as it is equal to 1.319 (for MO) and 1.680 (for MB), respectively.

3.5.3 Dubinin-Radushkevich (D-R) model

Dubinin-Radushkevich model [48] pointed out that the physical or chemical nature of the adsorption process, which is related to the hierarchical porous structure of the sorbent. This model can be expressed as:

$$ln q_e = -\beta \varepsilon^2 + ln q_m \qquad \text{(Eq.10)}$$

$$\varepsilon = RT ln\left(1 + {}^{1}/C_e\right) \qquad \text{(Eq.11)}$$

where $\beta$ (mol$^2$ J$^{-2}$) is the activity coefficient related to adsorption mean free energy; $\varepsilon$ is the Polanyi potential; $R$ is the gas constant (8.314 J mol$^{-1}$ K$^{-1}$); $T$ (K) is the absolute temperature.

418    The mean free energy of adsorption $E$ (kJ mol$^{-1}$) can be calculated to estimate the type of sorption process

419    using the following equation [49]:

420    $$E = 1/\sqrt{2\beta}$$ (Eq.12)

421    When $E$ is less than 8 kJ mol$^{-1}$, dyes removal belongs to physisorption process. While, 8-16 kJ mol$^{-1}$ ($E$)

422    implies the synergy of electrostatic interaction and chemisorption. If $E$ exceeds 16 kJ mol$^{-1}$, chemisorption

423    becomes the dominant process.

424    The D-R isotherm plot is shown in **Fig.11c**. The calculated values of $E$ were 8.606 kJ mol$^{-1}$ and 11.330 kJ mol$^{-1}$

425    for MO and for MB adsorption, respectively, demonstrating that azo-dyes removal by CCGMs was under the

426    synergy of electrostatic interaction and chemisorption, which was consistent with previous conclusions [50].
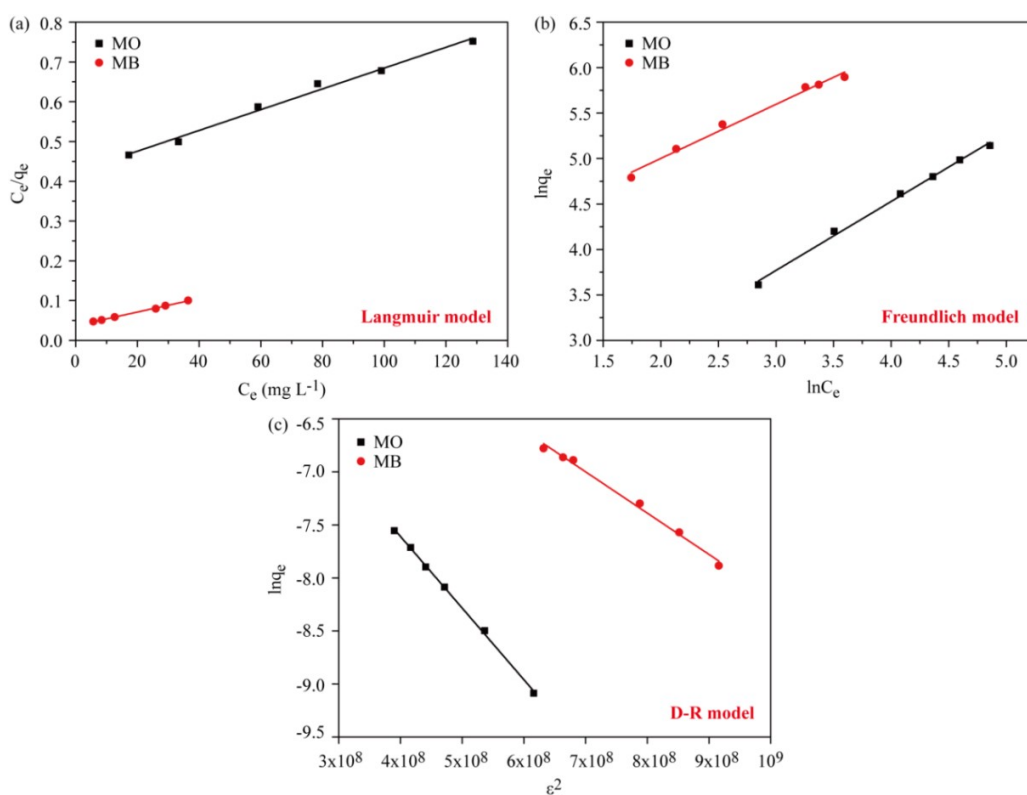


427

428    **Fig.11** The linear fitting curves of (a) Langmuir adsorption isotherm; (b) Freundlich adsorption isotherm; (c)

429                D-R adsorption isotherm, respectively.

430           **Table 3.** Parameters of adsorption isotherm models for MB and MO adsorption.

| Isotherm models | MO (pH=3, 30 °C) Parameters | | | MB (pH=11, 60 °C) Parameters | | |
|---|---|---|---|---|---|---|
| **Langmuir model** | $q_m$ (mg g$^{-1}$) | $k_L$ (L mg$^{-1}$) | $R^2$ | $q_m$ (mg g$^{-1}$) | $k_L$ (L mg$^{-1}$) | $R^2$ |
| | 383.142 | 6.166E-3 | 0.995 | 584.795 | 4.629E-2 | 0.998 |
| **Freundlich model** | $b$ | $k_F$ (g mg$^{-1}$) | $R^2$ | $b$ | $k_F$ (g mg$^{-1}$) | $R^2$ |
| | 1.319 | 4.458 | 0.988 | 1.680 | 45.178 | 0.986 |
| **D-R model** | $q_m$ (mol g$^{-1}$) | $\beta$ (mol$^2$ kJ$^{-2}$) | $R^2$ | $q_m$ (mol g$^{-1}$) | $\beta$ (mol$^2$ kJ$^{-2}$) | $R^2$ |

|  |  |  |  |  |  |
|---|---|---|---|---|---|
| 7.382E-3 | 6.751E-3 | 0.989 | 1.394E-2 | 3.895E-3 | 0.991 |

431 The maximum adsorption capacity of CCGMs towards MO and MB was calculated to be 383.142 mg g$^{-1}$ and

432 584.795 mg g$^{-1}$ at optimum adsorption conditions, significantly higher than that of the reported carboxymethyl

433 chitosan-based adsorbents in previous literatures (see **Table 4**). Therefore, it can be concluded that CCGMs

434 have good potential for the removal of cationic and anionic azo-dyes from aqueous solutions.

435

436 <mark>Table 4.</mark> Comparison of maximum adsorbance of different carboxymethyl chitosan-based adsorbents for MB

437 and MO dyes.

| Dyes | Adsorbents | Maximum adsorbance (q$_m$, mg g$^{-1}$) | Equilibrium time (t, h) | Optimum adsorption condition | |
|---|---|---|---|---|---|
|  |  |  |  | Temperature (°C) | pH |
| MB | N,O-carboxymethyl-chitosan[33] | 349 | 1 | 30 | 8 |
|  | Crosslinked Carboxymethyl-chitosan[51] | 342.6 | 2 | 25 | 5.6 |
|  | Carboxymethyl chitosan-modified magnetic-cored dendrimer[30] | 96.31 | < 1 | 25 | 11 |
|  | Crosslinked poly(vinyl alcohol)/carboxymethyl chitosan hydrogels for removal of metal ions and dyestuff from aqueous solutions[52] | 7 | 24 | 25 | NA |
|  | N,O-carboxymethyl chitosan[53] | 64.56 | NA | NA | ≥5 |
|  | CCGMs (**This work**) | 584.795 | 2 | 60 | 11 |
| MO | Carboxymethyl chitosan-modified magnetic-cored dendrimer[30] | 20.85 | < 1 | 25 | 3 |
|  | N,O-carboxymethyl chitosan[53] | 92.51 | NA | NA | ≤ 3 |
|  | Graphene oxide nanosheets/ carboxymethyl chitosan/ Fe$_3$O$_4$ magnetic composite microspheres[32] | 163.2 | 1.5 | 30 | 5.5 |
|  | CCGMs (**This work**) | 383.142 | < 1 | 30 | 3 |

438

439 3.6 Thermodynamic analysis

440 The influence of temperature is a main factor aspect in the adsorption process. The thermodynamic parameters,

441 such as standard free energy change ($\Delta G^0$, kJ mol$^{-1}$), standard enthalpy change ($\Delta H^0$, kJ mol$^{-1}$) and standard

442 entropy change ($\Delta S^0$, J mol$^{-1}$ K$^{-1}$), could be used to represent the adsorption heat and spontaneity of adsorption

443 behavior of the interaction between azo-dyes and CCGMs. All of the parameters above could be calculated

444 with the following equations [54].

$$\Delta G^0 = \Delta H^0 - T\Delta S^0 \qquad \text{(Eq.13)}$$

$$\Delta G^0 = -RT ln K_d \qquad \text{(Eq.14)}$$

447  Where $T$ is the temperature in (K) and $R$ is the real gas constant (8.314 J mol$^{-1}$ K$^{-1}$) the equilibrium constant $K_d$

448  (L g$^{-1}$) is determined by multiplying the Langmuir constants $q_m$ and $k_L$ ($K_d = q_m \times k_L$).

449  With using Eq.13 and Eq.14, the value of $\Delta H^0$ and $\Delta S^0$ were given from the intercept and slope of a plot of $\Delta G^0$

450  versus $T$, respectively [54]. The adsorption behaviors of CCGMs for MO and MB under different temperature

451  conditions were dispersed in Fig.12. Besides, all of these thermodynamic parameters were listed in **Table 5**.

452  The negative values of $\Delta G^0$ suggest that the adsorption processes are thermodynamically feasible and

453  spontaneous. However, The calculated $\Delta H^0$ were -8.312 kJ mol$^{-1}$ for MO and 25.285 kJ mol$^{-1}$ for MB,

454  respectively, indicating that the nature of adsorption behavior for MO and MB are exothermic and endothermic,

455  respectively. In addition, positive value of $\Delta S^0$ for MB, 103.301 J mol$^{-1}$ K$^{-1}$, indicates an irregular increase of

456  the randomness at the solid-solution interface during the fixation of adsorbates on the active sites of the

457  adsorbent. In this regard, the negative value of $\Delta S^0$ for MO, -20.230 J mol$^{-1}$ K$^{-1}$, demonstrates the opposite

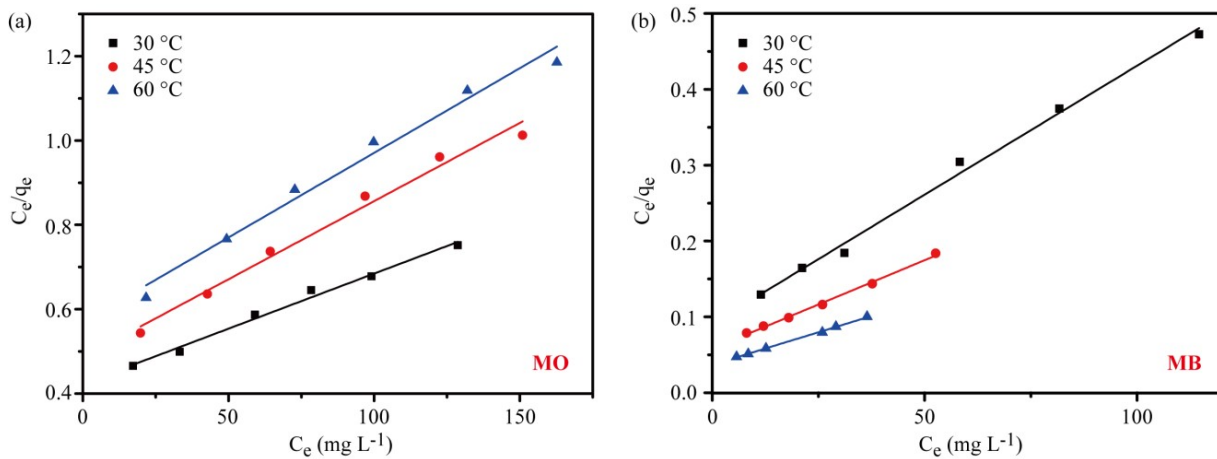458  irregular decrease property.

459



460  **Fig.12** The linear fitting by Langmuir equation for (a) MO and (b) MB at different adsorption temperatures,

461  respectively.

462

463  **Table 5.** Thermodynamic parameters for the adsorption of MO and MB on CCGMs.

|  | $T$ (°C) | $k_L$ (L mg$^{-1}$) | $q_m$ (mg g$^{-1}$) | $lnK_d$ | $\Delta G^0$(kJ mol$^{-1}$) | $\Delta H^0$(kJ mol$^{-1}$) | $\Delta S^0$(J mol$^{-1}$ K$^{-1}$) |
|---|---|---|---|---|---|---|---|
| **MO** | 30 | 6.166E-3 | 383.142 | 0.860 | -2.166 | | |
| | 45 | 7.639E-3 | 269.542 | 0.722 | -1.909 | -8.312 | -20.230 |
| | 60 | 7.042E-3 | 249.377 | 0.563 | -1.559 | | |
| **MB** | 30 | 3.728E-2 | 294.118 | 2.395 | -6.033 | | |
| | 45 | 4.016E-2 | 429.185 | 2.847 | -7.527 | 25.285 | 103.301 |
| | 60 | 4.629E-2 | 584.795 | 3.298 | -9.132 | | |

464

465  **4. Conclusion**

Novel CCGMs adsorbents were successfully synthesized by a facile inverse suspension route with two-step successive crosslinking process. MB and MO were chosen as the representatives of cationic and anionic azo-dyes to evaluate the selectivity property of as-prepared CCGMs. Various influential factors such as solution pH, temperature, and contact time were considered to ascertain the optimal condition for different azo-dyes adsorption. As a result, the maximum adsorbance of CCGMs for MO and MB at the optimized condition (pH=3 and 30 °C for MO, while pH=11 and 60 °C for MB) were 383.142 mg g$^{-1}$ and 584.795 mg g$^{-1}$, respectively. However, the required equilibrium time for MO adsorption was less than half of that for MB adsorption (2 h). Besides, it has been demonstrated that the pseudo-second order model was more suitable in explicating adsorption kinetics, while adsorption isotherms was fitting well with Langmuir model. Combining with the FT-IR and XPS curves, it can be concluded that the pH induced adsorption could be realized by the synergistic effect of electrostatic interaction and π-π stacking between dyes and CCGMs. Furthermore, the outstanding and stable regeneration of as-prepared CCGMs (re-adsorption efficiency of CCGMs for MO and MB were more than 80%) were also be verified with five consecutive recycling. Therefore, benefit from biodegradable and economic raw materials, coupled with facile synthesis route, the newly developed CCGMs could be a highly promising candidate for highly toxic dyestuff wastewater treatment.

**Appendix A. Supplementary data**

Supplementary data associated with this article can be found in **SI**.

**References**

[1] X. He, K.B. Male, P.N. Nesterenko, D. Brabazon, B. Paull, J.H.T. Luong, Adsorption and Desorption of Methylene Blue on Porous Carbon Monoliths and Nanocrystalline Cellulose, ACS Applied Materials & Interfaces, 5 (2013) 8796-8804.

[2] Y. Feng, H. Zhou, G. Liu, J. Qiao, J. Wang, H. Lu, L. Yang, Y. Wu, Methylene blue adsorption onto swede rape straw (Brassica napus L.) modified by tartaric acid: Equilibrium, kinetic and adsorption mechanisms, Bioresource Technology, 125 (2012) 138-144.

[3] D.-W. Cho, B.-H. Jeon, C.-M. Chon, F.W. Schwartz, Y. Jeong, H. Song, Magnetic chitosan composite for adsorption of cationic and anionic dyes in aqueous solution, Journal of Industrial and Engineering Chemistry,

499    28 (2015) 60-66.

500    [4] Y. Wang, G. Xia, C. Wu, J. Sun, R. Song, W. Huang, Porous chitosan doped with graphene oxide as highly

501    effective adsorbent for methyl orange and amido black 10B, Carbohydrate Polymers, 115 (2015) 686-693.

502    [5] S. Zhao, F. Zhou, L. Li, M. Cao, D. Zuo, H. Liu, Removal of anionic dyes from aqueous solutions by

503    adsorption of chitosan-based semi-IPN hydrogel composites, Composites Part B: Engineering, 43 (2012) 1570-

504    1578.

505    [6] N. Tripathy, R. Ahmad, H. Kuk, D.H. Lee, Y.-B. Hahn, G. Khang, Rapid methyl orange degradation using

506    porous ZnO spheres photocatalyst, Journal of Photochemistry and Photobiology B: Biology, 161 (2016) 312-

507    317.

508    [7] P.K. Malik, Dye removal from wastewater using activated carbon developed from sawdust: adsorption

509    equilibrium and kinetics, Journal of Hazardous Materials, 113 (2004) 81-88.

510    [8] C.A. Martínez-Huitle, E. Brillas, Decontamination of wastewaters containing synthetic organic dyes by

511    electrochemical methods: A general review, Applied Catalysis B: Environmental, 87 (2009) 105-145.

512    [9] L. Di, H. Yang, T. Xian, X. Liu, X. Chen, Photocatalytic and Photo-Fenton Catalytic Degradation

513    Activities of Z-Scheme Ag2S/BiFeO3 Heterojunction Composites under Visible-Light Irradiation,

514    Nanomaterials, 9 (2019) 399.

515    [10] M.A. Shannon, P.W. Bohn, M. Elimelech, J.G. Georgiadis, B.J. Mariñas, A.M. Mayes, Science and

516    technology for water purification in the coming decades, Nature, 452 (2008) 301-310.

517    [11] W. Cheah, S. Hosseini, M.A. Khan, T.G. Chuah, T.S.Y. Choong, Acid modified carbon coated monolith

518    for methyl orange adsorption, Chemical Engineering Journal, 215-216 (2013) 747-754.

519    [12] C.-H. Wu, Adsorption of reactive dye onto carbon nanotubes: Equilibrium, kinetics and thermodynamics,

520    Journal of Hazardous Materials, 144 (2007) 93-100.

521    [13] S. Deng, H. Xu, X. Jiang, J. Yin, Poly(vinyl alcohol) (PVA)-Enhanced Hybrid Hydrogels of

522    Hyperbranched Poly(ether amine) (hPEA) for Selective Adsorption and Separation of Dyes, Macromolecules,

523    46 (2013) 2399-2406.

524    [14] A.-H. Chen, S.-M. Chen, Biosorption of azo dyes from aqueous solution by glutaraldehyde-crosslinked

525    chitosans, Journal of Hazardous Materials, 172 (2009) 1111-1121.

526    [15] F. Zhao, E. Repo, D. Yin, Y. Meng, S. Jafari, M. Sillanpää, EDTA-Cross-Linked β-Cyclodextrin: An

527    Environmentally Friendly Bifunctional Adsorbent for Simultaneous Adsorption of Metals and Cationic Dyes,

528    Environmental Science & Technology, 49 (2015) 10570-10580.

529    [16] J. Fu, Q. Xin, X. Wu, Z. Chen, Y. Yan, S. Liu, M. Wang, Q. Xu, Selective adsorption and separation of

530    organic dyes from aqueous solution on polydopamine microspheres, Journal of Colloid and Interface Science,

23

461 (2016) 292-304.

[17] Y. Shen, Q. Fang, B. Chen, Environmental Applications of Three-Dimensional Graphene-Based Macrostructures: Adsorption, Transformation, and Detection, Environmental Science & Technology, 49 (2015) 67-84.

[18] C. Zhou, S. Lee, K. Dooley, Q. Wu, A facile approach to fabricate porous nanocomposite gels based on partially hydrolyzed polyacrylamide and cellulose nanocrystals for adsorbing methylene blue at low concentrations, Journal of Hazardous Materials, 263 (2013) 334-341.

[19] G. Crini, P.-M. Badot, Application of chitosan, a natural aminopolysaccharide, for dye removal from aqueous solutions by adsorption processes using batch studies: A review of recent literature, Progress in Polymer Science, 33 (2008) 399-447.

[20] L. Fan, C. Luo, X. Li, F. Lu, H. Qiu, M. Sun, Fabrication of novel magnetic chitosan grafted with graphene oxide to enhance adsorption properties for methyl blue, Journal of Hazardous Materials, 215-216 (2012) 272-279.

[21] M.-S. Chiou, H.-Y. Li, Equilibrium and kinetic modeling of adsorption of reactive dye on cross-linked chitosan beads, Journal of Hazardous Materials, 93 (2002) 233-248.

[22] B. Wang, Y. Zhu, Z. Bai, R. Luque, J. Xuan, Functionalized chitosan biosorbents with ultra-high performance, mechanical strength and tunable selectivity for heavy metals in wastewater treatment, Chemical Engineering Journal, 325 (2017) 350-359.

[23] B. Wang, Z. Bai, H. Jiang, P. Prinsen, R. Luque, S. Zhao, J. Xuan, Selective heavy metal removal and water purification by microfluidically-generated chitosan microspheres: Characteristics, modeling and application, Journal of Hazardous Materials, 364 (2019) 192-205.

[24] Y. Wang, X. Liu, H. Wang, G. Xia, W. Huang, R. Song, Microporous spongy chitosan monoliths doped with graphene oxide as highly effective adsorbent for methyl orange and copper nitrate (Cu(NO3)2) ions, Journal of Colloid and Interface Science, 416 (2014) 243-251.

[25] C.-Y. Chen, J.-C. Chang, A.-H. Chen, Competitive biosorption of azo dyes from aqueous solution on the templated crosslinked-chitosan nanoparticles, Journal of Hazardous Materials, 185 (2011) 430-441.

[26] L. Zhou, J. Jin, Z. Liu, X. Liang, C. Shang, Adsorption of acid dyes from aqueous solutions by the ethylenediamine-modified magnetic chitosan nanoparticles, Journal of Hazardous Materials, 185 (2011) 1045-1052.

[27] W. Zhao, X. Huang, Y. Wang, S. Sun, C. Zhao, A recyclable and regenerable magnetic chitosan absorbent for dye uptake, Carbohydrate Polymers, 150 (2016) 201-208.

[28] W.S. Wan Ngah, L.C. Teong, M.A.K.M. Hanafiah, Adsorption of dyes and heavy metal ions by chitosan

composites: A review, Carbohydrate Polymers, 83 (2011) 1446-1456.

[29] X. Wang, X. Ma, Z. Yang, Z. Zhang, J. Wen, Z. Geng, Z. Wang, An NBD-armed tetraaza macrocyclic lysosomal-targeted fluorescent probe for imaging copper(ii) ions, Chemical Communications, 49 (2013) 11263-11265.

[30] H.-R. Kim, J.-W. Jang, J.-W. Park, Carboxymethyl chitosan-modified magnetic-cored dendrimer as an amphoteric adsorbent, Journal of Hazardous Materials, 317 (2016) 608-616.

[31] M. Zhang, Y. Zhang, R. Helleur, Selective adsorption of Ag+ by ion-imprinted O-carboxymethyl chitosan beads grafted with thiourea–glutaraldehyde, Chemical Engineering Journal, 264 (2015) 56-65.

[32] S. Lv, L. Zhu, Y. Li, C. Jia, S. Sun, The Adsorption Capacity of GONs/CMC/Fe$_3$O$_4$ Magnetic Composite Microspheres and Applications for Purifying Dye Wastewater, Materials, 10 (2017) 58-69.

[33] L. Wang, Q. Li, A. Wang, Adsorption of cationic dye on N,O-carboxymethyl-chitosan from aqueous solutions: equilibrium, kinetics, and adsorption mechanism, Polymer Bulletin, 65 (2010) 961-975.

[34] L. Yue, L. Zhang, H. Zhong, Carboxymethyl chitosan: A new water soluble binder for Si anode of Li-ion batteries, Journal of Power Sources, 247 (2014) 327-331.

[35] A.K. Gupta, M. Gupta, S.J. Yarwood, A.S.G. Curtis, Effect of cellular uptake of gelatin nanoparticles on adhesion, morphology and cytoskeleton organisation of human fibroblasts, Journal of Controlled Release, 95 (2004) 197-207.

[36] S. Bensalem, B. Hamdi, S. Del Confetto, M. Iguer-Ouada, A. Chamayou, H. Balard, R. Calvet, Characterization of chitosan/montmorillonite bionanocomposites by inverse gas chromatography, Colloids and Surfaces A: Physicochemical and Engineering Aspects, 516 (2017) 336-344.

[37] E. Zheng, Q. Dang, C. Liu, B. Fan, J. Yan, Z. Yu, H. Zhang, Preparation and evaluation of adipic acid dihydrazide cross-linked carboxymethyl chitosan microspheres for copper ion adsorption, Colloids and Surfaces A: Physicochemical and Engineering Aspects, 502 (2016) 34-43.

[38] Y.A. Azarova, A.V. Pestov, A.Y. Ustinov, S.Y. Bratskaya, Application of chitosan and its N-heterocyclic derivatives for preconcentration of noble metal ions and their determination using atomic absorption spectrometry, Carbohydrate Polymers, 134 (2015) 680-686.

[39] W. Luo, Z. Bai, Y. Zhu, Comparison of Co(ii) adsorption by a crosslinked carboxymethyl chitosan hydrogel and resin: behaviour and mechanism, New Journal of Chemistry, 41 (2017) 3487-3497.

[40] W.S. Wan Ngah, L.C. Teong, R.H. Toh, M.A.K.M. Hanafiah, Comparative study on adsorption and desorption of Cu(II) ions by three types of chitosan–zeolite composites, Chemical Engineering Journal, 223 (2013) 231-238.

[41] A. Riga, K. Soutsas, K. Ntampegliotis, V. Karayannis, G. Papapolymerou, Effect of system parameters

and of inorganic salts on the decolorization and degradation of Procion H-exl dyes. Comparison of H2O2/UV, Fenton, UV/Fenton, TiO2/UV and TiO2/UV/H2O2 processes, Desalination, 211 (2007) 72-86.

[42] Y. Dong, L. He, Q. Wang, M. Yang, R. Qi, K. Li, Effect of inorganic salts on ferric oxalate-induced decomposition of CI Acid Black 234 under different weather conditions, Coloration Technology, 124 (2008) 19-26.

[43] H.Y. Zhu, R. Jiang, Y.Q. Fu, J.H. Jiang, L. Xiao, G.M. Zeng, Preparation, characterization and dye adsorption properties of γ-Fe2O3/SiO2/chitosan composite, Applied Surface Science, 258 (2011) 1337-1344.

[44] W.J. Weber, J.C. Morris, Kinetics of Adsorption on Carbon From Solution, Asce Sanitary Engineering Division Journal, 1 (1963) 1-2.

[45] H. Tajizadegan, O. Torabi, A. Heidary, M.H. Golabgir, A. Jamshidi, Study of methyl orange adsorption properties on ZnO–Al2O3 nanocomposite adsorbent particles, Desalination and Water Treatment, 57 (2016) 12324-12334.

[46] K.K.H. Choy, J.F. Porter, G. McKay, Langmuir Isotherm Models Applied to the Multicomponent Sorption of Acid Dyes from Effluent onto Activated Carbon, Journal of Chemical & Engineering Data, 45 (2000) 575-584.

[47] H.M.F. Freundlich, Over the adsorption in solution, Journal of Physical Chemistry, 57 (1906) 385-470.

[48] M.M. Dubinin, E.D. Zaverina, L.V. Radushkevich, Sorption and structure of active carbons. I. Adsorption of organic vapors, Russian Journal of Bioorganic Chemistry, 21 (1947) 1351-1362.

[49] J. Karuga, Y.A.C. Jande, H.T. Kim, C.K. King'Ondu, Fish Swim Bladder-Derived Porous Carbon for Defluoridation at Potable Water pH, Advances in Chemical Engineering & Science, 06 (2016) 500-514.

[50] J. Fan, Z. Zhao, W. Liu, Y. Xue, S. Yin, Solvothermal synthesis of different phase N–TiO2 and their kinetics, isotherm and thermodynamic studies on the adsorption of methyl orange, Journal of Colloid and Interface Science, 470 (2016) 229-236.

[51] B. Doshi, A. Ayati, B. Tanhaei, E. Repo, M. Sillanpää, Partially carboxymethylated and partially cross-linked surface of chitosan versus the adsorptive removal of dyes and divalent metal ions, Carbohydrate Polymers, 197 (2018) 586-597.

[52] M.W. Sabaa, R.R. Mohamed, S.H. Eltaweel, R.S. Seoudi, Crosslinked poly(vinyl alcohol)/carboxymethyl chitosan hydrogels for removal of metal ions and dyestuff from aqueous solutions, Journal of Applied Polymer Science, 123 (2012) 3459-3469.

[53] M. Wu, Y. Bai, W. Li, D. Xu, W. Chen, H. Ma, Facile synthesis of pH-sensitive carboxymethyl chitosan and its tunable adsorption property toward anionic and cationic dyes, Desalination and Water Treatment, 126 (2018) 333-344.

627    [54] G.R. Mahdavinia, A. Massoudi, A. Baghban, E. Shokri, Study of adsorption of cationic dye on magnetic

628    kappa-carrageenan/PVA nanocomposite hydrogels, Journal of Environmental Chemical Engineering, 2 (2014)

629    1578-1587.

630

631